International Journal of Computer Assisted Radiology and Surgery (2019) 14:321–333
https://doi.org/10.1007/s11548-018-1887-3

ORIGINAL ARTICLE

A robotic microsurgical forceps for transoral laser microsurgery

Manish Chauhan[1] · Nikhil Deshpande[2] · Claudio Pacchierotti[3] · Leonardo Meli[4] · Domenico Prattichizzo[2,4] · Darwin G. Caldwell[2] · Leonardo S. Mattos[2]

Received: 23 April 2018 / Accepted: 6 November 2018 / Published online: 21 November 2018

Abstract

Purpose In transoral laser microsurgery (TLM), the close curved cylindrical structure of the laryngeal region offers functional challenges to surgeons who operate on its malignancies with rigid, single degree-of-freedom (DOF) forceps. These challenges include surgeon hand tremors, poor reachability, poor tissue surface perception, and reduced ergonomy in design. The integrated robotic microsurgical forceps presented here is capable of addressing the above challenges through tele-operated tissue manipulation in TLM.

Methods The proposed device is designed in compliance with the spatial constraints in TLM. It incorporates a novel 2-DOF motorized microsurgical forceps end-effector, which is integrated with a commercial 6-DOF serial robotic manipulator. The integrated device is tele-operated through the haptic master interface, Omega.7. The device is augmented with a force sensor to measure tissue gripping force. The device is called RMF-2F, i.e. robotic microsurgical forceps with 2-DOF end-effector and force sensing. RMF-2F is evaluated through validation trials and pick-*n*-place experiments with subjects. Furthermore, the device is trialled with expert surgeons through preliminary tasks in a simulated surgical scenario.

Results RMF-2F shows a motion tracking error of less than 400 μm. User trials demonstrate the device's accuracy in task completion and ease of manoeuvrability using the Omega.7 through improved trajectory following and execution times. The tissue gripping force shows better regulation with haptic feedback (1.624 N) than without haptic feedback (2.116 N). Surgeons positively evaluated the device with appreciation for improved access in the larynx and gripping force feedback.

Conclusions RMF-2F offers an ergonomic and intuitive interface for intraoperative tissue manipulation in TLM. The device performance, usability, and haptic feedback capability were positively evaluated by users as well as expert surgeons. RMF-2F introduces the benefits of robotic teleoperation including, (i) overcoming hand tremors and wrist excursions, (ii) improved reachability and accuracy, and (iii) tissue gripping feedback for safe tissue manipulation.

Keywords Robot-assisted microsurgical forceps · Robotic teleoperation · Tissue gripping haptic feedback · Robotic medical instruments · Minimally invasive surgery · Transoral laser microsurgery

Introduction

Transoral laser microsurgery (TLM) is a non-invasive surgery for the treatment of laryngeal malignancies, e.g. cysts, polyps, nodules, or cancerous tumours. Introduced by Jako et al. [1], the traditional technique, as seen in Fig. 1a, involves inserting a laryngoscope (length = 180 mm, cross-section 16×23 mm^2) into the patient's mouth to expose the surgical site. This allows a direct line-of-sight for the surgical microscope. A laser micro-manipulator, consisting of a beam-splitter mirror and a small mechanical joystick, is coupled to the surgical microscope. The free-beam CO_2 surgical laser is aimed manually at the site by moving the mirror.

✉ Nikhil Deshpande
nikhil.deshpande@iit.it

1 STORM Lab, School of Electronics and Electrical Engineering, University of Leeds, Leeds LS2 9JT, UK

2 Department of Advanced Robotics, Istituto Italiano di Tecnologia, Via Morego 30, 16163 Genoa, Italy

3 Centre National de la Recherche Scientifique (CNRS), Rainbow Team, Irisa and Inria Rennes Bretagne Atlantique, 35000 Rennes, France

4 Department of Information Engineering and Mathematics, Università degli Studi di Siena, Via Roma 56, 53100 Siena, Italy

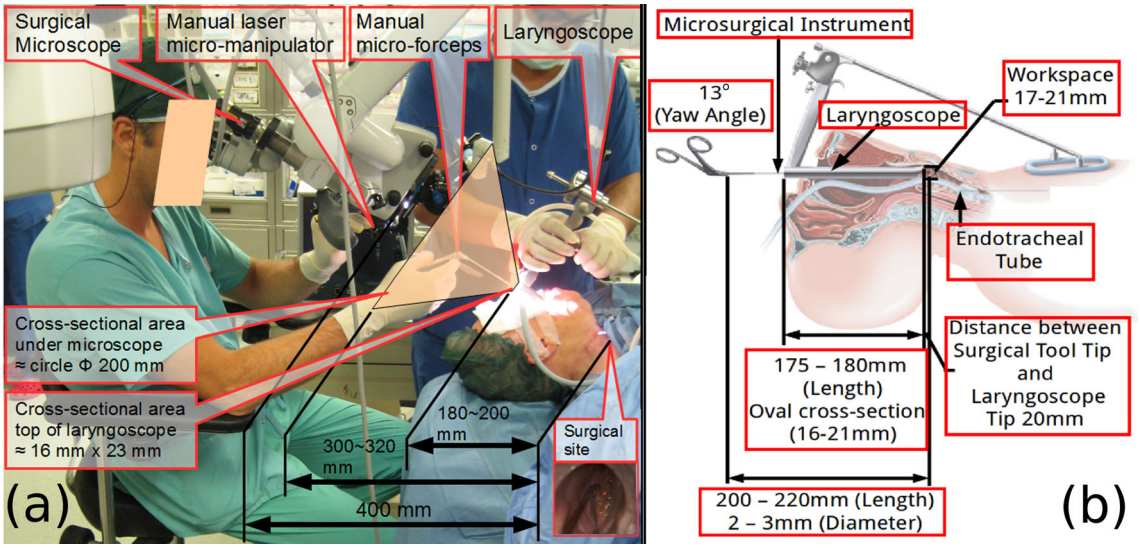

Fig. 1 Traditional TLM surgical setup: **a** overall dimensions; **b** dimensions around the laryngoscope

Additionally, manually handled microsurgical instruments allow intraoperative tissue manipulation and extraction.

Problem formulation

The manual microsurgical instruments in traditional TLM have scissor-like handles for open-close operation. The most common instrument, the microsurgical forceps (micro-forceps), is used for: (i) tissue manipulation (grasping, orienting, removing); (ii) stretching tissue for precise laser cutting and ensuring minimal thermal damage to healthy tissue; and (iii) orienting tissue to view pathologies. Figure 1b shows the dimensions of the various components within the TLM setup. As is seen, within the standard 400 mm laser focal distance between the base of the microscope and the surgical site, a narrow 50–100 mm range is available for inserting and manoeuvring the micro-forceps. Furthermore, these tools being rigid shaft cause: (i) constrained accessibility in the laryngeal region; (ii) unstable handling due to hand tremors and wrist excursions; and (iii) poor tissue gripping perception. This makes their usage cumbersome and non-ergonomic [2, 3].

To overcome the above-mentioned limitations, robotic assistance has been introduced in laryngeal surgery [4]. Towards this end, Simaan et al. [5] presented snake-like manipulators having tip dexterity for tissue manipulation and suturing. Wang et al. [6] presented a robot-assisted master–slave system consisting of two symmetrical 9 degrees-of-freedom (DOFs) cable-driven manipulators, with quick-change interfaces for surgical tools. Solares and Strome [7] and Desai et al. [8] explored the utility of the *da Vinci Surgical System* [4] but found the size of the *da Vinci* tool shafts as a major limitation. These endeavours seek to replace the microscope with dedicated instrument arms entering through the laryngoscope. Importantly, although targeted at laryngeal surgery, the above systems cannot be used in TLM, since there would be no available access for the free-beam laser. He et al. [9] overcame this drawback through their cooperatively controlled teleoperation robot. In this approach, the instruments can be directly attached/detached from the 3-DOF wrist of the robot itself. Their design serves as an important guidepost for the research in this paper.

On a related note, tissue haptic perception is widely considered to be valuable for robot-assisted surgical procedures, showing enhanced perception accuracy, decreased completion times, and decreased peak and mean applied forces [10]. In TLM, given that the thickness of the laryngeal tissue is about 3–5 mm [1], especially in the vocal cords, the regulation of tissue gripping forces is critical in avoiding tissue trauma or rupture. The lack of gripping force feedback is also a limitation with He et al. [9].

With the above background, the goal of this article is the introduction of robotic micro-forceps in TLM with a suitable haptic handling interface.

Contributions

Previously, in [11], the authors presented a first robotic micro-forceps prototype, which was bulky and unusable under the TLM microscope. In [12], a second version was designed, having a motorized 1-DOF end-effector, which complied with the constraints of TLM and was integrated with a force sensor. Its haptic master interface provided teleoperation control through gesture scaling and elimination of hand tremors

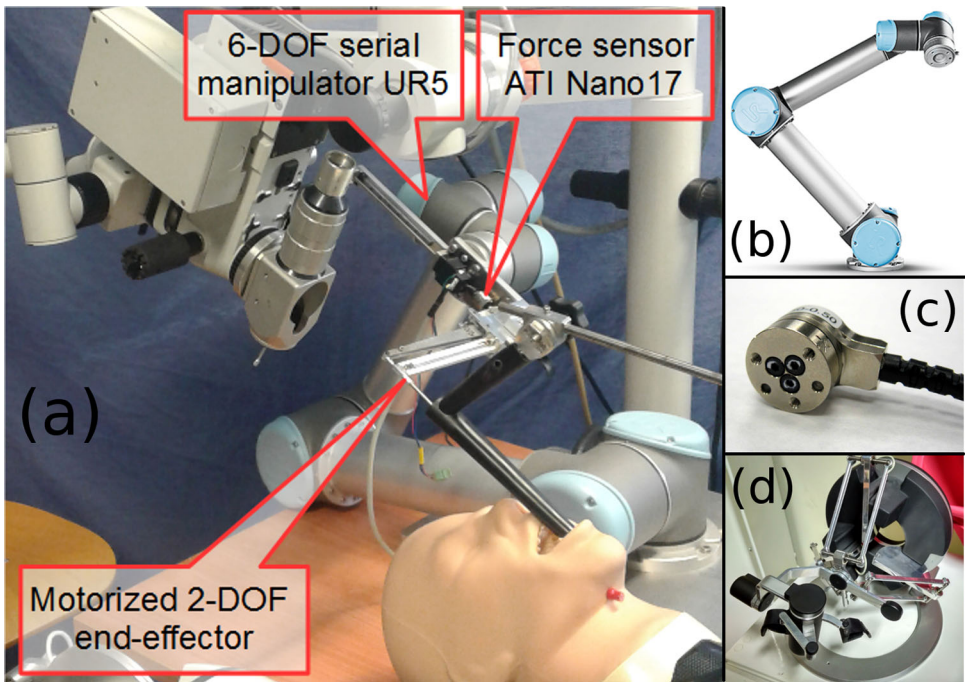

Fig. 2 The 5-DOF "RMF-2F" device. **a** 2-DOF micro-forceps end-effector integrated with the 6-DOF UR5 robot and the ATI Nano17 force sensor; **b** UR5; **c** ATI Nano17; **d** Omega.7

and wrist excursions [12]. The haptic feedback facilitated better regulation of gripping force application [12]. Taking this previous research forward, this article presents the design of an improved version of the robotic micro-forceps device, having:

(i) a motorized 2-DOF micro-forceps end-effector, with gripper jaw open/close and tool shaft rotation for enhanced reachability. The previous version in [12] was only 1-DOF;
(ii) teleoperation control similar to [11];
(iii) tissue gripping force (TGF) capability with impedance-based feedback (as opposed to proportional feedback [12]) for improved tissue surface perception; and
(iv) updated experimental evaluation including phantom tissue-based test bed along with preliminary validation with expert surgeons, which was not done in [12].

The 2-DOF end-effector, integrated with a commercial 6-DOF serial manipulator arm (UR5 [13]) and the force sensor (ATI Nano17 [14]), forms the RMF-2F, i.e. robotic microsurgical forceps with 2-DOF end-effector and force feedback, as seen in Fig. 2a. The device is configured to be a 5-DOF setup: 3-DOF Cartesian positioning at the surgical site combined with the 2-DOF end-effector. The RMF-2F is controlled by a haptic master device under unilateral teleoperation through the Omega.7 haptic master interface [15]. The following sections discuss the design, analysis, and evaluation of the proposed device.

Design of the motorized 2-DOF micro-forceps end-effector

Figure 1b points to the key dimensions in TLM, while Table 1 lists the key features, which are considered in the design of the motorized 2-DOF end-effector. The values for these features are arrived at empirically through measurements of the traditional setup and discussions with expert surgeons. Any mechanism to be used under the microscope, in-line with the surgical line-of-sight, and parallel to the laser beam, would need to have a small thickness to avoid vision occlusion and interference with the laser. Consequently, any actuators for the motorized DOFs would have to be placed away from the line-of-sight. Features 1 and 2 in the Table are therefore, derived from the dimensional constraints of TLM.

The main components of the 2-DOF micro-forceps are the: (i) tool shaft, (ii) tool shaft holder, and (iii) tool actuation mechanism.

The tool shaft

The traditional tool shaft has an outer diameter of $\phi = 2$ mm with an inner translating wire (*itw*, $\phi = 1$ mm). The translation of this wire by 3 mm (determined experimentally) provides the open-close DOF for the tool jaws. To adapt it, the proximal end of the shaft is modified by attaching a hollow extension tube with external M3 threading to it. This modification is termed as the docking interface (DI) (refer Fig. 3). The *itw* passes through the hollow DI to attach to the

Table 1 Design specifications of the microsurgical forceps

Design needs/features	Remarks
Displacement from microscope line-of-sight of 200 mm	To minimize vision occlusion and avoid tool interference with laser path, sufficient distance between the laryngoscope entry point and the designed tool base is necessary
Tool cross-section under the microscope of < 10 mm	To maintain minimum vision occlusion, when viewed through the microscope
Introduce tissue surface perception through haptic feedback	To receive tissue gripping force feedback
Introduce tool rotation DOF	Enhance tool capability for enhanced workspace and reachability

tool actuation mechanism for the open/close DOF, while the outer shaft attaches to the tool shaft holder.

The tool shaft holder

Figure 4 shows the design of the tool shaft holder, which supports the tool shaft as well as the tool actuation mechanism. It comprises of three sub-frames: $F1$, $F2$, and $F3$. A housing, H_S, mounted on $F1$ at $P1$, supports the tool shaft. H_S houses two small ball bearings B_f and B_r. The DI is held within the bearings to incorporate the rotational DOF. H_S is designed to have a cross-sectional thickness of 8 mm.

The sub-frames $F1$ and $F2$ are rigidly connected at $P2$. The sub-frame $F3$ supports the linear actuator driving the open/close DOF while $F2$ supports the rotary motor providing the rotational DOF. The mechanisms are explained in the following subsections.

The tool actuation mechanism

The tool actuation mechanism has two main components: the *Open/Close DOF* and the *Rotational DOF*.

Open/close DOF

This mechanism is adopted directly from the design in [12]. Figure 5 shows the mechanism consisting of five linkages ($L1$, $L2$, $L3$, $L4$, $L5$), designed to provide linear translation of the *itw*. The hinge link $L1$ is considered as ground. $L2$ forms the input link along the actuator axis and it transfers direct motion to $L3$, which in-turn transfers inverse motion to $L4$ about $L1$. $L4$ is directly coupled to the driven link $L5$, which is attached to the *itw*. The Nanotec L2018 linear actuator, with 30 N feed force, drives the open/close DOF.

The detailed mechanism design using the graphical synthesis method is presented in [12]. There are two key insights in the design:

(i) The force sensor is located at $L2$ with its measurement axis coincident with the actuator axis. The reaction force of the closing of the forceps on tissue is transmitted through the *itw* and the linkages on to the sensor surface, which in-turn outputs a signal in direct proportion to the gripping action.
(ii) As stated in Table 1, the optimal displacement between the tool base and the microscope line-of-sight is 200 mm. Here, through the choices of 50 mm and

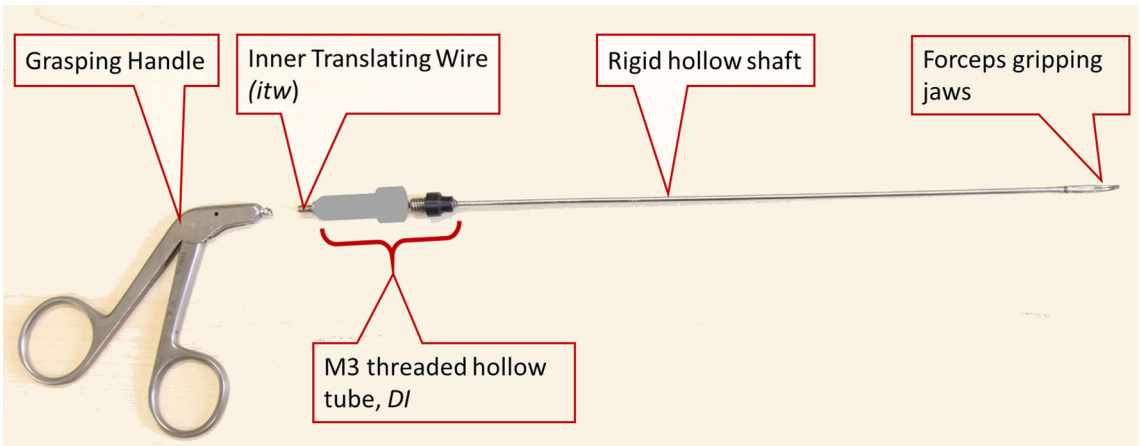

Fig. 3 The tool shaft

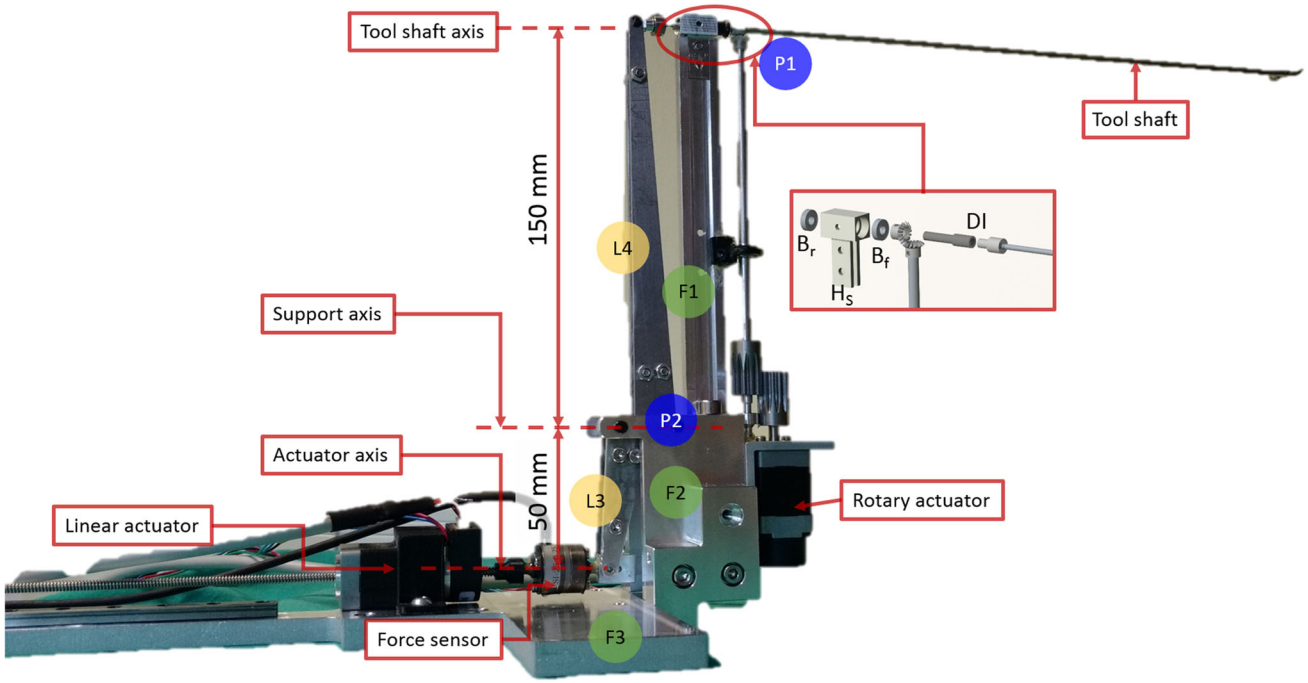

Fig. 4 The tool shaft holder

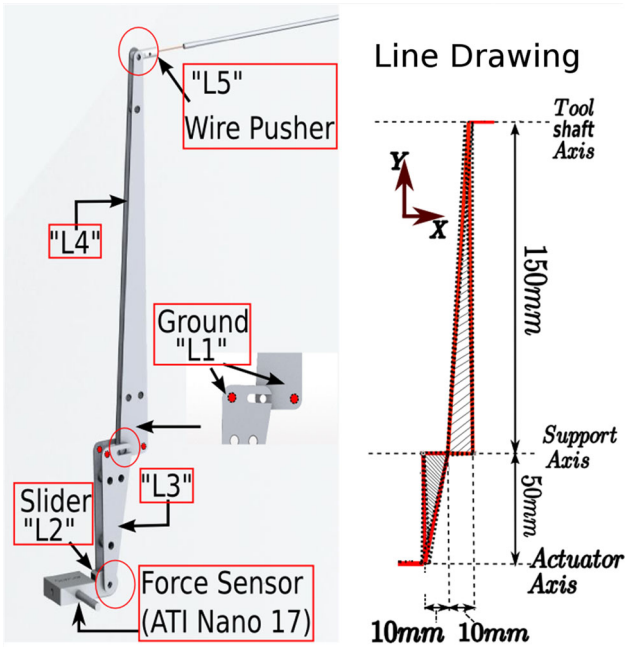

Fig. 5 The tool actuation mechanism

150 mm for the lengths of $L3$ and $L4$, the total distance between the tool shaft axis and the actuator axis becomes 200 mm. Additionally, the link-length ratio for $L4$:$L3$ becomes 3:1. Thus, a 1 mm displacement of $L2$ results in a 3 mm displacement of $L5$ and the *itw*, resulting in the open/close of the micro-forceps jaws.

Rotational DOF

The mechanism for the rotational DOF is implemented as the coordinated motion of three components: (i) miter gear assembly (MG); (ii) spur gear assembly (SG); and (iii) modified link $L5$ mechanism (M_{L5}) (refer Fig. 6).

(i) *Miter Gear assembly*, (*MG*) The tool shaft rotation is made possible through a miter gear assembly with an outer diameter[1] of 8 mm (refer Fig. 6a). The gear G_O is mounted onto a shaft S_O such that it is orthogonal to the tool shaft axis. The axial gear G_A is mounted co-axially with the tool shaft axis and attaches rigidly to the DI of the tool shaft. The miter gear assembly G_O-to-G_A transfers rotation to the tool shaft through DI.

(ii) *Spur Gear assembly*, (*SG*) The shaft S_O rotates through a low-backlash 1:1 spur gear assembly (SG_1 and SG_2) (refer Fig. 6b). This assembly transfers the rotary motion of the actuator (R_M, Nanotec SC2018 with 1.8 N-cm torque) to S_O, and thereby to *MG*. An additional ball bearing (B_b) supports the rotation of S_O and reduces the vibrations in the rotation.

(iii) *Modified link L5 in the open/close DOF*, (M_{L5}) To allow simultaneous rotation and translation of the *itw* (through the DI), a suitable adaptation is necessary in link $L5$. Three components are introduced for this purpose: (i) a specially designed holder (H_I) with set-

[1] This is within the H_S thickness of 8 mm.

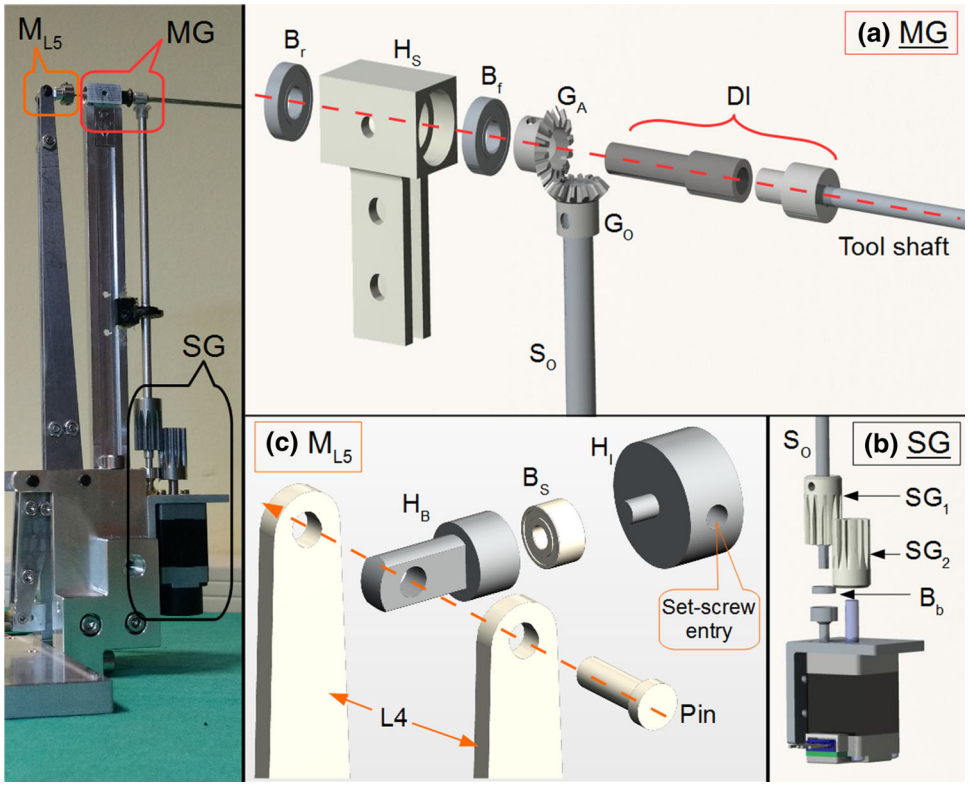

Fig. 6 Detailed view of the rotational DOF of the tool actuation mechanism. **a** miter gear assembly, (MG); **b** spur gear assembly, (SG); **c** link L5 modification, (M_{L5})

Table 2 *D–H* parameters for the RMF-2F integrated device

Joint	Type	a (m)	α (radians)	d (m)	q (radians)
1	*R*	0.00000	$\pi/2$	$d_1 = 0.089159$	q_1
2	*R*	−0.42500	0.0	0.0000	q_2
3	*R*	−0.39225	0.0	0.0000	q_3
4	*F*	0.00000	$\pi/2$	$d_4 = 0.10915$	0
5	*F*	0.00000	$-\pi/2$	$d_5 = 0.09465$	0
6	*F*	0.00000	0.0	$d_6 = 0.0823 + l_6$	0
7	*R*	0.00000	$\pi/2$	$d_7 = 0.108 + l_7$	q_{rot}

R rotary, *F* fixed, $l_6 = 210$ mm, $l_7 = 200$ mm are dimensions of micro-forceps, q_{rot} rotary DOF

screws to attach the *itw*. The holder includes a small shaft extension; (ii) this extension is inserted into a small ball bearing (B_S), thereby allowing H_1 to rotate freely; (iii) B_S is held within a housing H_B which is integrated with link *L*4 (refer Fig. 6c).

With these adaptations, the motorized micro-forceps has 2-DOFs in compliance with the TLM constraints.

Integration of the robotic micro-forceps-RMF-2F

As seen in Fig. 2, the 2-DOF motorized micro-forceps tool is attached as an end-effector to the UR5 robotic manipulator at a 90^o angle, resulting in the RMF-2F device. The UR5, seen in Fig. 2b, has a payload capacity of 5 kg, repeatability of 0.1 mm, a reach radius of 850 mm, and can be controlled at 125 Hz. These values make it suitable for precise teleoperation control. Since the motorized micro-forceps already has a rotational DOF, the final orientation DOF of the UR5 is not used. The *D–H* parameters of the integrated RMF-2F device are suitably updated as a 5-DOF global device (3-DOF positioning + 1 DOF rotation + 1 DOF open/close), as given in Table 2.

Teleoperation control and validation

A master haptic interface, the force dimension Omega.7, as seen in Fig. 2d, teleoperates the RMF-2F. The Omega.7 has 7-DOFs (6-DOF motion + 1-DOF gripper), of which the

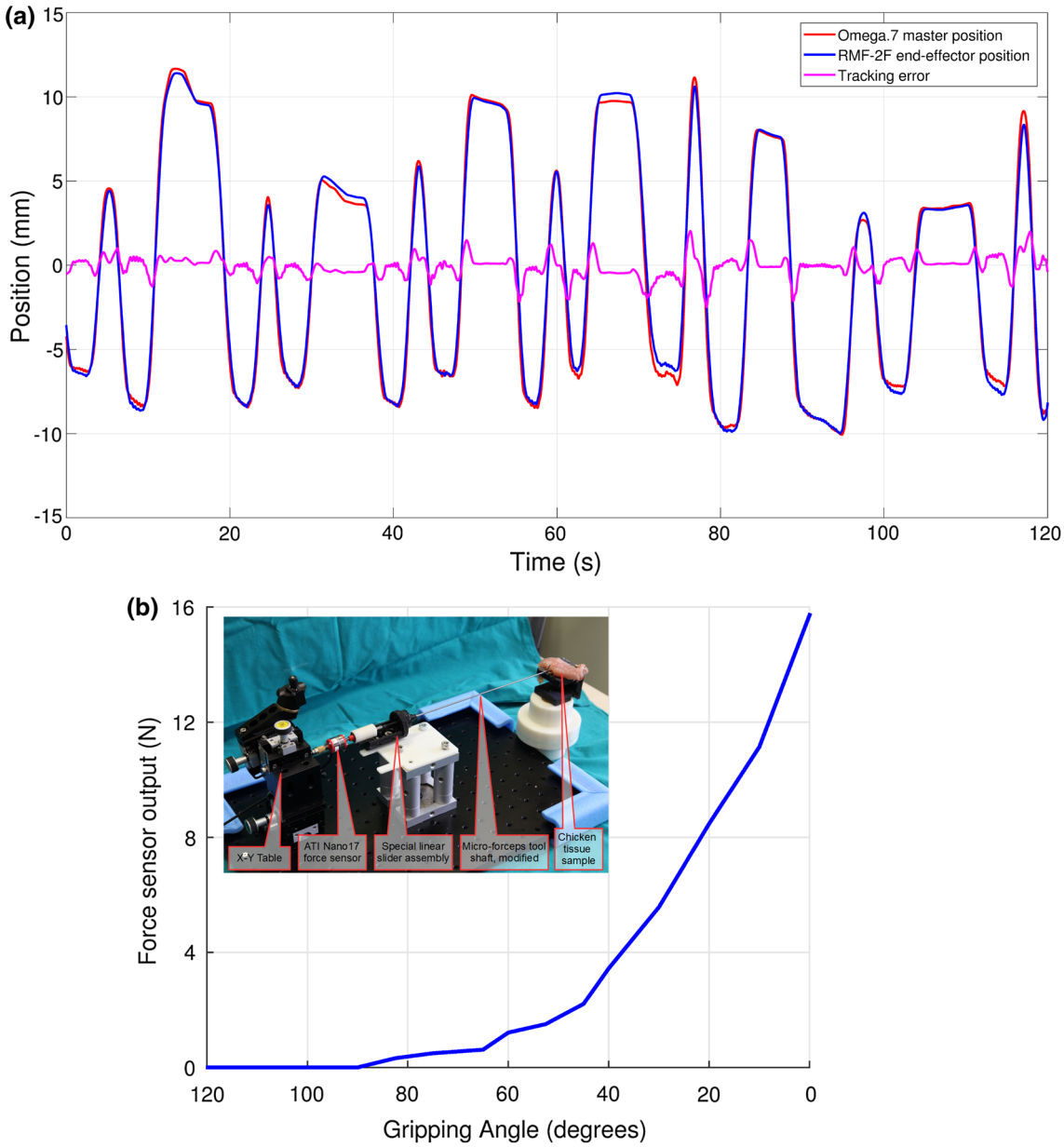

Fig. 7 Characterization of the RMF-2F: **a** motion control evaluation; **b** TGF sensing (inset: characterization setup)

three translational DOFs and the gripper DOF are active. The three translational DOFs control the 3-DOF positioning of the RMF-2F. The *yaw* DOF of the Omega.7 commands the rotational DOF of the RMF-2F, while the gripper DOF commands its open/close. Omega.7 provides active gravity compensation to improve the teleoperation transparency and reduce the operator's fatigue. The integrated system uses a dedicated gigabit Ethernet connection between the master and the RMF-2F device, ensuring minimal time delay between the two. A two-layer, time-domain controller [16] preserves the stability and transparency of the system.

(i) Since the kinematics of the master interface and the RMF-2F are non-homothetic, a unilateral velocity-based teleoperation controller is implemented. This was suitable for the requirements of the narrow workspace inside the laryngoscope. The 3-DOF master end-effector velocity $\left(\dot{q}_h \in \mathbb{R}^3\right)$ is filtered and scaled with a gesture scaling factor ζ and mapped to the velocity $\left(\dot{q}_r \in \mathbb{R}^3\right)$ of the RMF-2F, as shown in Eq. 1. The constants have values: $\zeta = 0.2$ and $\beta = 0.025$, adapted from [11]

$$\begin{aligned} \dot{q}_h^k &= (1-\beta)\cdot \dot{q}_h^{k-1} + \beta \cdot \dot{q}_h \\ \dot{q}_r^k &= J^{-1}\cdot \dot{q}_h^k \cdot \zeta \end{aligned} \tag{1}$$

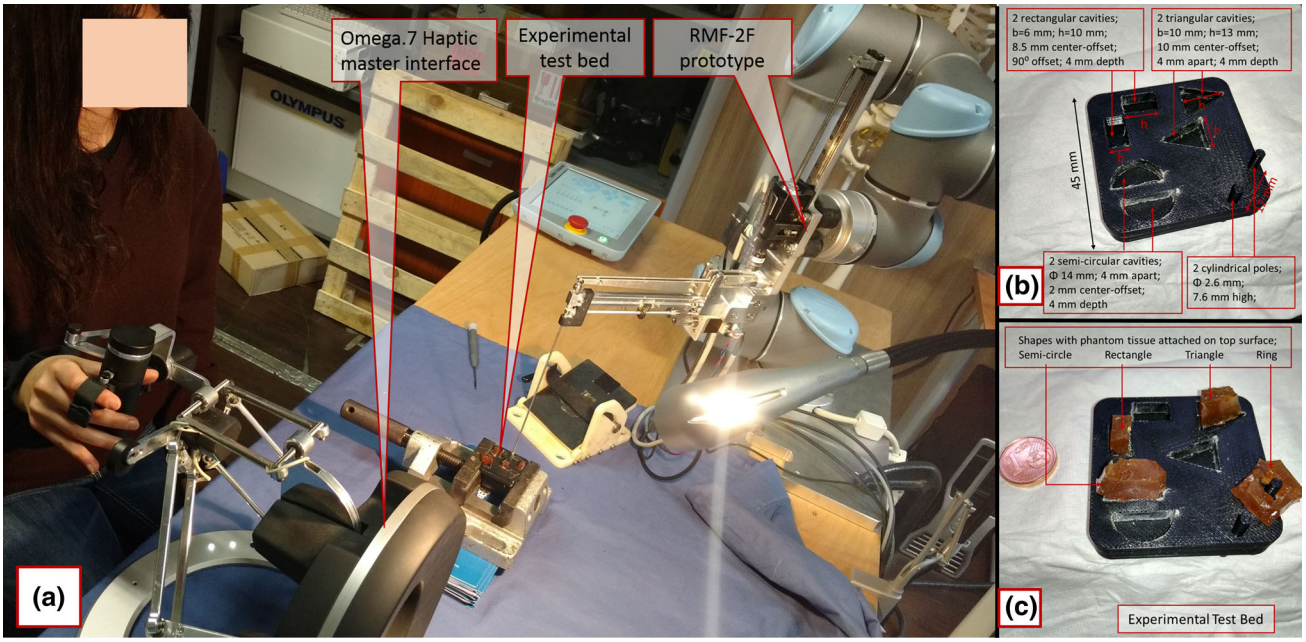

Fig. 8 Experimental evaluation setup. **a** Subject performing trial; **b** test bed dimensions; **c** test bed with phantom tissue shapes

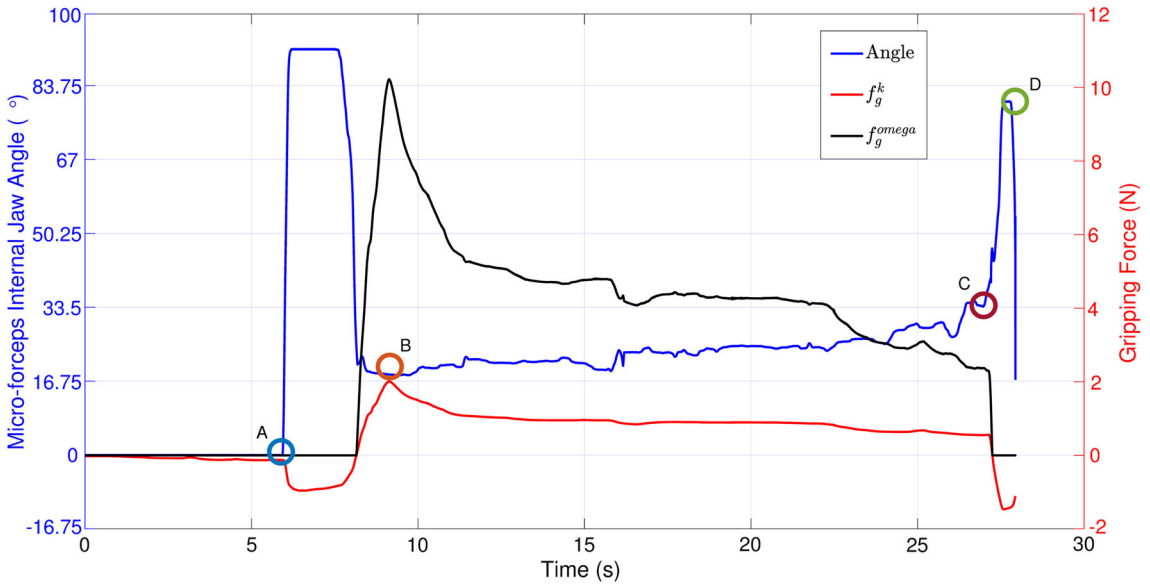

Fig. 9 Sample trial depicting behaviour of Eq. 5. The highlighted locations indicate the phases of the trial: '*A*' micro-forceps opening; '*B*' shape gripped; '*C*' shape release initiated; '*D*' shape release completed

J^{-1} is the inverse of the manipulator Jacobian matrix, $J \in \mathbb{R}^{3x3}$. The integrated system was characterized in [11] giving a low position mapping error of 0.3901 mm $\pm$ 0.3829 mm, signifying transparency and accuracy. Figure 7a shows a sample plot for the tracking error in one axis.

(ii) For the end-effector, the jaw open/close and tool-tip rotation are controlled unilaterally. The relationship is shown by Eq. 2, where $\eta_1 = 3$ and $\eta_2 = 2$ are empirically chosen to compensate for the friction and hysteresis in the system. The position command loop runs at 100 Hz

$$\begin{bmatrix} q_{\text{rot}} \\ q_{\text{jaw}} \end{bmatrix} = \begin{bmatrix} \eta_1 & 0 \\ 0 & \eta_2 \end{bmatrix} \begin{bmatrix} q_{\text{h}}^{\text{yaw}} \\ q_{\text{h}}^{\text{grip}} \end{bmatrix}. \quad (2)$$

For force sensing, the ATI Nano17 Force/Torque sensor (Fig. 2c, $\phi = 17$ mm, $L = 14.5$ mm) offers a fine resolution of 3.125 mN with sensing up to 70 N, and registering data at 7 kHz. The characterization of the TGF at the sensor was done

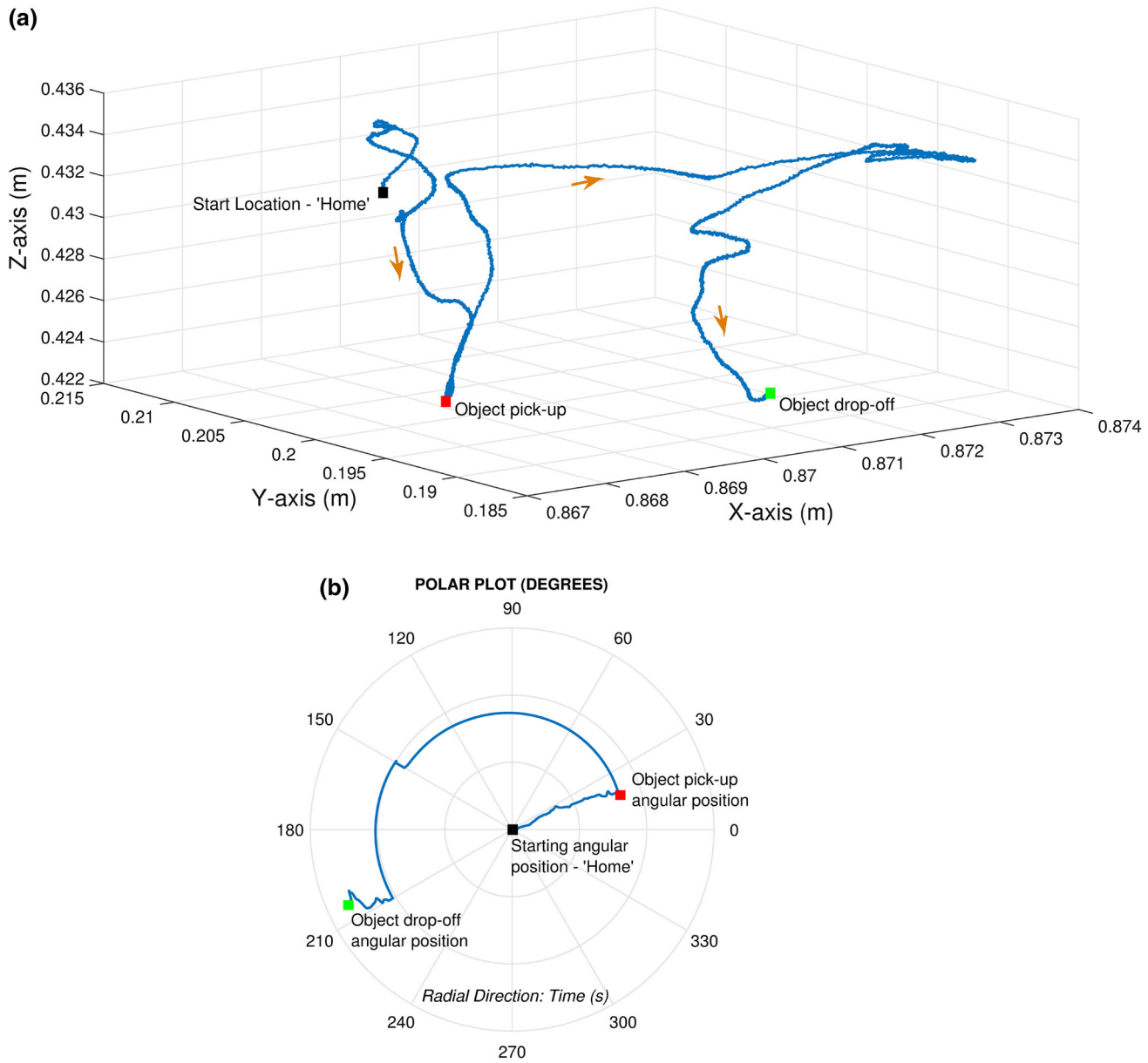

Fig. 10 RMF-2F trajectory during a sample trial. **a** 3-DOF position during task; **b** angular orientation during task

in [11]. Figure 7b shows the TGF value varying nonlinearly from the fully open position of the micro-forceps (0 N, tissue not touching the jaws) to the fully closed position (16 N). The inset in Fig. 7b shows the customized characterization setup.

Experimental evaluation

The performance of the RMF-2F device was validated through evaluation experiments simulating real surgical actions like grasping, pulling, and manipulating the laryngeal tissue. These trials were performed with 10 non-medical subjects (mean age = 28.2 years; 8 males, 2 females) with no prior experience in such tasks. The trials consisted of pick-rotate-*n*-place tasks, as seen in Fig. 8. A test bed with cavities for different 3D-printed shapes (triangle, rectangle, semi-circle, and circular ring) was prepared. The shapes were fixed with artificial tissue-like material to provide tissue gripping sensation. This phantom tissue is a bi-component polyurethane elastomer (F-105 A/B 5 shore, BJB Enterprise) added with a softening agent (SC-22, BJB Enterprise) [17]. For uniformity of results, each trial began with the RMF-2F in home position (15 mm above the test bed centre). The experiments were conducted in two conditions, $C1$ (haptic feedback activated) versus $C2$ (haptic feedback deactivated).

In condition $C1$, the measured TGF is rendered to the gripper DOF of Omega.7. To do this, the force sensor value is first filtered using a low-pass filter ($\beta = 0.001$, Eq. 3), to suppress

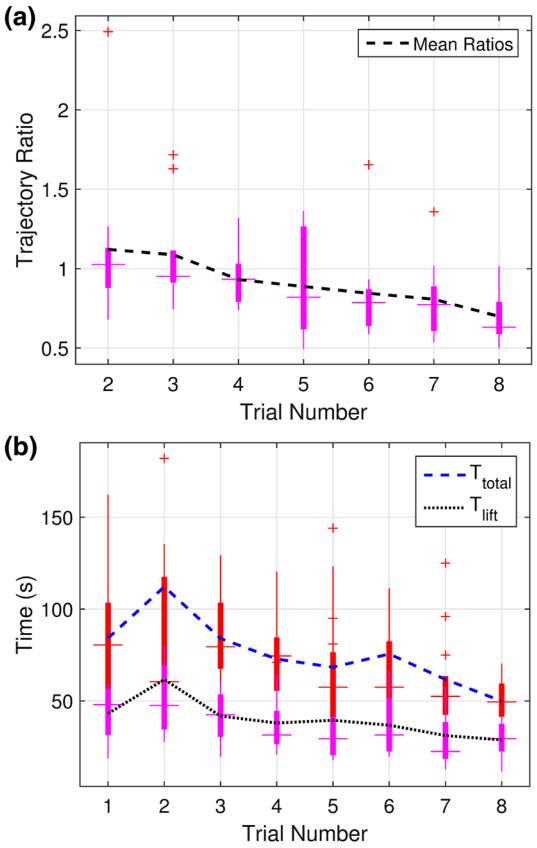

Fig. 11 Results of experimental evaluation. **a** Overall trajectory ratio; **d** execution time

noisy signals. It is then scaled based on the internal angle of the micro-forceps jaws using Eq. 4. The value rendered to the gripper DOF is calculated using Eq. 5. Here, Ω_g is the maximum internal angle of the jaws in open position, i.e. 90°, and ω_g^k is the internal angle at instant k. After extensive offline testing, the values of the constants were obtained as $c = 1.5$ and $\gamma = 1/20$, giving $1.5 < k^k < 5.5$. The rendered force therefore varies in proportion to the sensed force as well as the internal angle of the gripping jaws, giving an impedance-based haptic feedback

$$f_g^k = (1-\beta)\cdot f_g^{k-1} + \beta \cdot f_g^{\text{sensor}} \tag{3}$$

$$k^k = \gamma.\left(\Omega_g - \omega_g^k\right) + c \tag{4}$$

$$f_g^{\text{omega}} = \begin{cases} 0, & f_g^k \le 0 \\ k^k \cdot f_g^k, & f_g^k > 0 \end{cases} \tag{5}$$

f_g^{sensor} is calibrated to avoid the values from the free-space open/close of the RMF-2F. The haptic feedback loop runs at 500 Hz to ensure transparency. Figure 9 shows the behaviour of Eq. 5 for ω_g^k, f_g^k, and f_g^{omega} with a sample trial with the Triangle shape. As is seen, f_g^k varies between -1 and 2 N, while f_g^{omega} varies between 0 and 10 N, through the various phases of: closed jaws (0° angle), micro-forceps opening (‘A’), shape gripped (‘B’), shape release initiated (‘C’), and shape released (‘D’).

Subjects conducted eight trials each (twice on each shape) in the following order: (i) Semi-circle, (ii) Ring, (iii) Triangle, and (iv) Rectangle. The conditions $C1$ and $C2$ were randomized across the trials to obtain un-biased evaluation. The device performance was analysed by measuring the: (i) trajectory followed by the RMF-2F for the tasks; (ii) execution time required to conduct the tasks; (iii) number of failed attempts during task execution; and (iv) TGF feedback performance in $C1$ and $C2$ conditions.

Trajectory analysis

Figure 10a shows a sample trajectory for the RMF-2F with the triangle shape, starting from the home position, picking-up the object from its cavity, and then placing it in the other cavity. The re-orientation of the objects during the trial is quantified (180° in case of the Triangle) in Fig. 10b, where the radial direction represents the time in seconds. For analysing the usability of the device, the trajectory ratio was used as a metric. With eight consecutive trials, the trajectory length for the first trial was used as the basis against which the ratios for the 7 succeeding trials were calculated. Figure 11a shows the overall trend of the ratios over time indicating that the subjects find the device easy and quick to learn. The ratio of the 8th-to-1st trial is 0.6988, while the average ratio over the 7 trials is 0.9111. The positive performance for the device is attributed to the ease-of-learning offered by the Omega.7 interface and its transparent integration with the RMF-2F.

Execution time and controllability

A similar downward trend in the time taken for the task completion demonstrates the RMF-2F's ease-of-learn-ability. Figure 11b shows such trends for the two metrics: (i) time to lift the shape from the cavity (T_{lift}); and (ii) time to transfer the shape (T_{total}). As observed, T_{lift} goes from 43.2 to 28.8 s, an improvement of 33.3%. The same trend is seen for T_{total}, going from 84.2 to 49.9 s, giving an improvement of almost 40%.

In terms of controllability, over all the trials (a total of 80), only 18 failed attempts (failure to lift the shape or transfer it to the other cavity) were recorded in task execution.

Tissue gripping force analysis

TGF feedback analysis was conducted using the f_g^k value from Eq. 5. Figure 12a shows a sample trial for the Triangle shape in the $C1$ and $C2$ conditions, where the difference in levels of force is evident. The highlighted locations indicate phases of the task. The analysis shows that the average

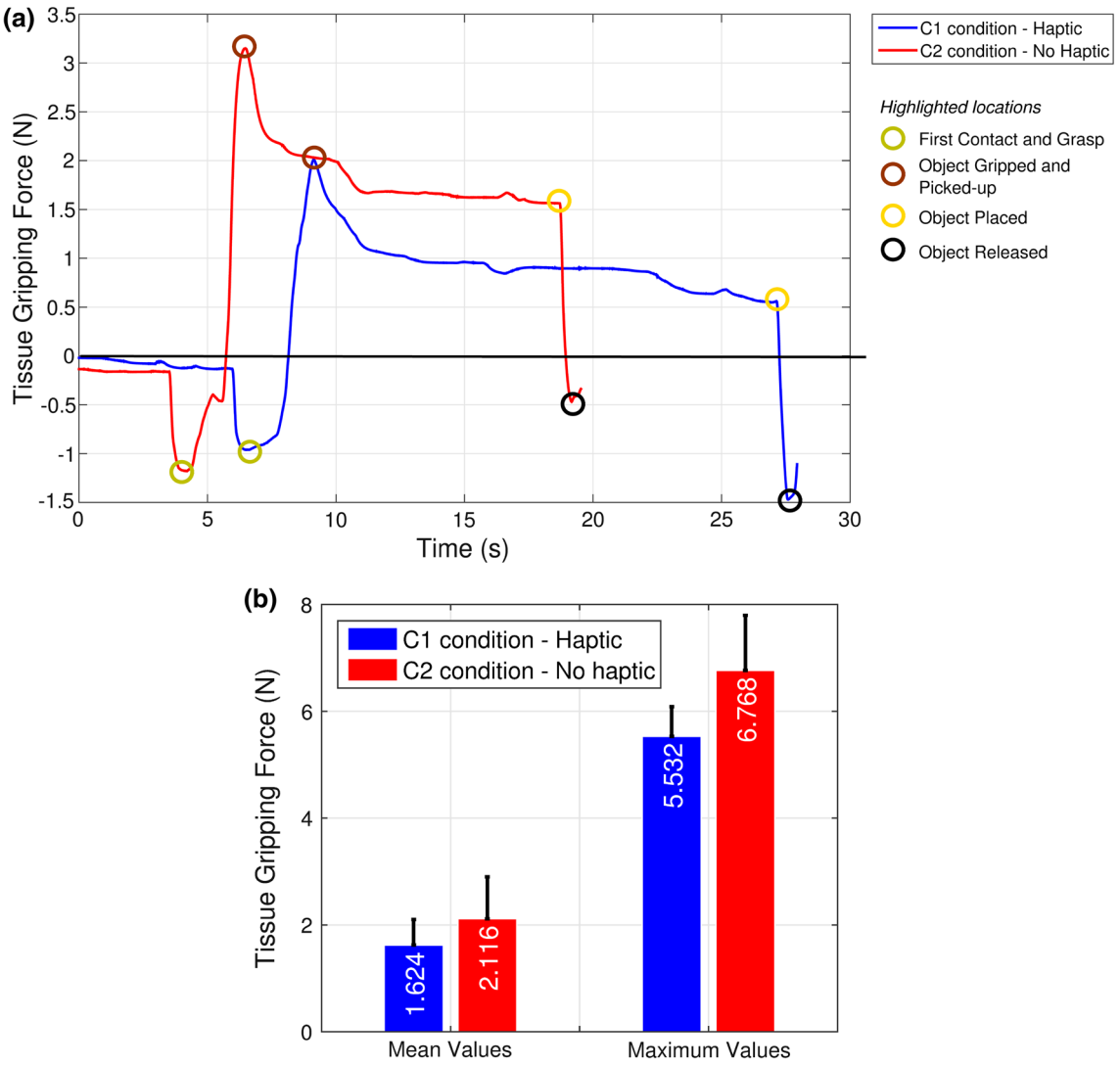

Fig. 12 Results of TGF analysis. **a** Difference in TGF values for $C1$ and $C2$ condition for a sample trial; **b** comparison of mean and maximum TGF

TGF applied on the phantom tissue is less in condition $C1$ (1.624 N) in comparison to $C2$ (2.116 N), as seen in Fig. 12b. This difference is statistically significant according to the *Student's t* test ($p = 0.0486$). Similarly, the value for the maximum TGF is less in $C1$ (5.532 N) than in $C2$ (6.768 N), although not statistically significant ($p > 0.05$). For soft tissue, the closing of the RMF-2F jaws displaces the tissue around the jaws, thereby causing a nonlinear variance (and reduction) in the gripping force over time. By incorporating the internal jaw angle in the force feedback, this effect of squeezing soft tissue can be compensated for, providing a more natural tissue gripping sensation. This demonstrates better regulation of gripping forces in the $C1$ condition, where the subjects applied less force on the phantom tissue, as against the $C2$ condition. It allows better tissue surface perception and improved safety against potential tissue trauma.

Furthermore, in terms of controllability, out of the 18 failed trials recorded, 8 were in the $C1$ condition and 10 in the $C2$ condition. Although positive for $C1$, this data is not conclusive enough.

Preliminary surgeon trials

To introduce RMF-2F in the TLM operating room (OR), it is important to understand the suitability of its functionality and features for the surgeons. In this regard, three surgeons from the Ospedale San Martino in Genova (Italy) were invited to perform preliminary experiments using the RMF-2F device. To simulate real surgery, ex vivo pig larynxes, held in a specially designed holder, were used. Pig larynxes, available at the supermarket, resemble the human larynx closely and surgeons use them frequently for training purposes [18]. The surgical setup, with surgical microscope, laryngoscope, laser

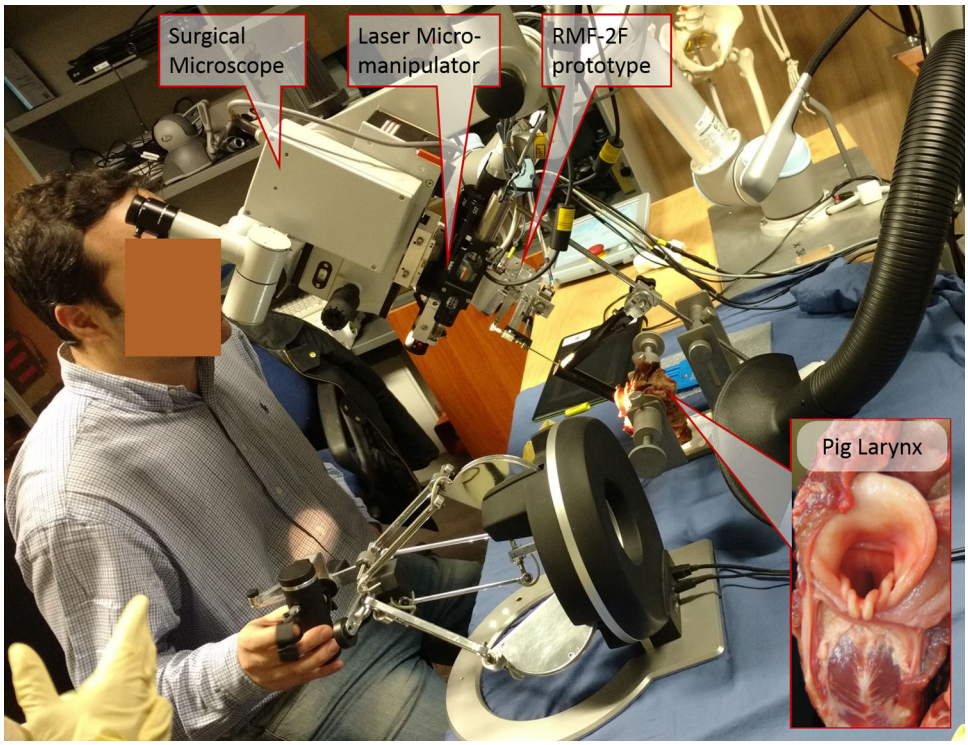

Fig. 13 Setup for preliminary trials of RMF-2F with expert surgeons

micro-manipulator, larynx-holder, and the RMF-2F, is seen in Fig. 13. When positioned properly, the pig larynx provides similar constraints as in the real TLM surgery, and thus is an optimal test bed to evaluate the overall RMF-2F design. The surgeons were asked to perform grasping, pulling, turning, and manipulation of the larynx tissue. The surgeons provided useful informal feedback:

(i) *Tool-tip rotation* This functionality was appreciated by the surgeons since it helped them reach different areas of the vocal region. They were able to grip-n-turn the tissue for better exposition.
(ii) *Appreciation of TGF feedback* While using the device under two different feedback conditions ($C1$ and $C2$), surgeons could distinguish between gripping action on tissues and regulate the applied forces.
(iii) *Vision occlusion under microscope* The surgeons complained about partial vision occlusion during usage. This implies the need to further reduce the device dimensions.

Discussion

The RMF-2F device is a first-of-its-kind device introducing robotic assistance and haptic feedback in TLM, while also complying with the associated spatial constraints. The positive evaluations from the non-medical subjects and surgeons demonstrate that the RMF-2F would be beneficial in the TLM OR. The ergonomics and comfort while controlling the device, tissue perception through haptic feedback, and reachability with the device are key improvements introduced by RMF-2F.

The evaluations pointed to the required improvements as well. The cantilever tool shaft introduced small vibrations at the tip and caused the vision occlusion mentioned by the surgeons. Based on comments by the surgeons, an additional DOF for tip articulation may would allow overcoming these issues through better tip control, while also enhancing accessibility. This re-design is currently under investigation.

The surgeon trials also highlighted the need for training in using a device like the RMF-2F, especially through haptic teleoperation. Years of prior training allows surgeons to use traditional manual tools under the microscope effortlessly. With similar experience, surgeons may be able to easily manoeuvre robotic devices through teleoperation as well.

Conclusions

This paper presented a novel design of the 5-DOF RMF-2F device for intraoperative use in TLM, integrated with the Omega.7 teleoperation haptic master and the ATI Nano17 force sensor. The RMF-2F device offers: (i) motorized tool-tip open/close and rotation; (ii) precise motion, stable positioning, no hand tremors, reduced wrist excursions, and gesture scaling through teleoperation; and (iii) improved safety through tissue gripping haptic feedback.

In future research, along with improvements in device form-factor, the gripping force shall be further investigated for isolating different components like stretching, twisting, etc. The limits of stability and transparency shall also be established for intuitiveness in robotic teleoperation.

Compliance with ethical standards

Conflict of interest The authors declare that they have no conflict of interest.

Ethical approval For this type of study, formal ethics approval was not required. The *Ethics Committee of Liguria Region* granted the exemption for the use of human subjects and ex vivo pig larynxes for the trials.

Informed consent Informed consent was obtained from all individual participants included in the study.

Site of research and experiments The research was carried out at the Istituto Italiano di Tecnologia (IIT) in Genova, Italy.

References

1. Jako GJ (1972) Laser surgery of the vocal cords: an experimental study with carbon-dioxide lasers on dogs. Laryngoscope 82(12):2204–2216
2. Liverneaux PA, Berner SH, Bednar MS, Parekattil SJ, Ruggiero GM, Selber JC (2012) Telemicrosurgery: robot assisted microsurgery. Springer, Paris
3. Hirano M (1974) Morphological structure of the vocal cord as a vibrator and its variations. Folia Phoniatr Logop 26(2):89–94
4. Da Vinci Surgical System (2018) Intuitive surgical. www.intuitivesurgical.com. Accessed on 30th Mar 2018
5. Simaan N, Taylor R, Flint P (2004) A dexterous system for laryngeal surgery. In: IEEE ICRA, pp 351–357
6. Wang S, Li Q, Ding J, Zhang Z (2006) Kinematic design for robot-assisted laryngeal surgery systems. IEEE/RSJ IROS:2864–2869
7. Solares CA, Strome M (2007) Transoral robot-assisted CO_2 laser supraglottic laryngectomy: experimental and clinical data. Laryngoscope 117(5):817–820
8. Desai SC, Sung CK, Jang DW, Genden EM (2008) Transoral robotic surgery using a carbon dioxide flexible laser for tumors of the upper aerodigestive tract. Laryngoscope 118(12):2187–2189
9. He C, Olds K, Iordachita I, Taylor R (2013) A new ENT microsurgery robot: error analysis and implementation. In: IEEE ICRA, pp 1221–1227
10. Van der Meijden O, Schijven M (2009) The value of haptic feedback in conventional and robot-assisted minimal invasive surgery and virtual reality training: a current review. Surg Endosc 23(6):1180–1190
11. Deshpande N, Chauhan M, Pacchierotti C, Prattichizzo D, Caldwell DG, Mattos LS (2016) Robot-assisted microsurgical forceps with haptic feedback for transoral laser microsurgery. In: IEEE EMBC, 38th edn. IEEE, pp 5156–5159
12. Chauhan M, Deshpande N, Barresi G, Pacchierotti C, Prattichizzo D, Caldwell DG, Mattos LS (2017) Design and control of a novel robotic microsurgical forceps for transoral laser microsurgery. In: IEEE AIM, pp 737–742
13. Univeral Robot (2018). www.universal-robots.com/products/ur5-robot. Accessed on 30th Mar 2018
14. ATI Nano17 Force Sensor (2018). www.ati-ia.com/Products/ft/ft_modelsaspx?id=Nano17. Accessed on 30th Mar 2018
15. Force Dimension Omega.7 (2018). www.forcedimension.com/products/omega-7/overview. Accessed on 30th Mar 2018
16. Franken M, Stramigioli S, Misra S, Secchi C, Macchelli A (2011) Bilateral telemanipulation with time delays: a two-layer approach combining passivity and transparency. IEEE Trans Rob 27(4):741–756
17. Ciullo A, Penza V, Mattos L, De Momi E (2016) Development of a surgical stereo endoscopic image dataset for validating 3D stereo reconstruction algorithms. In: CRAS workshop, 6th edn, pp 62–63
18. Jiang JJ, Raviv JR, Hanson DG (2001) Comparison of the phonation related structures among pig, dog, white-tailed deer, and human larynges. Ann Otol Rhinol Laryngol 110(12):1120–1125